RESEARCH PAPER

Quantitative Imaging Techniques for Osteoporosis: Current Status, Advances, and Future Directions

Mr. Pratap Singh[1*], Mr. Ravi Christian[1], Mr. Khush Jain[1], Ms. Nilofer Neshat[1], Mr. Lalramdinmawia Ralte[1], Ms. Shrawani Sonewane[1], Mr. Shubham Gupta[2]

[1]Assistant Professor, Department of Medical Radiology, Imaging and Therapeutic Technology, Parul Institute of Allied and Healthcare Sciences, Parul University, Vadodara, Gujarat, India – 391760
[2]Associate Professor and Head, Department of Medical Radiology, Imaging and Therapeutic Technology, Parul Institute of Allied and Healthcare Sciences, Parul University, Vadodara, Gujarat, India – 391760

Corresponding Author
Mr. Pratap Singh

How to cite this article: Singh P, Christian R, Jain K, Neshat N, Ralte L, Sonewane S, Gupta S. Quantitative Imaging Techniques for Osteoporosis: Current Status, Advances, and Future Directions. Int J Drug Deliv Technol. 2026;16(35s): 864-885. DOI: 10.25258/ijddt.16.35s.95

INTRODUCTION

Osteoporosis leads to decreased bone density and quality, heightening the risk of fragile fractures. It is a critical global health issue that contributes to significant morbidity and mortality while placing a substantial burden on healthcare systems, particularly in ageing populations.(1)

Standard methods for assessing fracture risk have relied on two main sources of information: clinical risk factors and bone mineral density measurement (BMD). The World Health Organization (WHO) developed the Fracture Risk Assessment Tool (FRAX®), a widely used algorithm to determine an individual's 10-year risk probability of major osteoporotic and hip fractures by using BMD and clinical factors, including age, sex, prior fracture history, and glucocorticoid use. The Garvan Fracture Risk Calculator provides users with an alternate method for estimating fracture risk probabilities. However, both assessment tools demonstrate particular sensitivity challenges, resulting in many individuals who sustain fragility fractures not being identified as high-risk before the occurrence of fractures. (1,2)

The primary method for diagnosing osteoporosis involves the assessment of bone mineral density using dual-energy X-ray absorptiometry (DXA). However, individuals with BMD values in the osteopenic or normal range sustain fractures at high rates, as BMD alone does not fully capture overall fracture risk. Conditions such as 2 diabetes mellitus and degenerative spinal disease further illustrate that fracture risk may increase when BMD remains stable or above normal levels. This is because bone strength depends on both bone mass and its structural factors, including microarchitecture, cortical geometry, tissue mineralization, collagen integrity and microdamage accumulation.(3,4)

In recent years, quantitative imaging has developed beyond the capabilities of DXA. The techniques such as quantitative computed tomography (QCT), high-resolution peripheral QCT (HR-pQCT), magnetic resonance imaging (MRI), quantitative ultrasound (QUS), positron emission tomography (PET), and the trabecular bone score (TBS) enables comprehensive evaluation of bone structure, which include cortical and trabecular compartments, 3D bone geometry, microstructural patterns, bone marrow composition and skeletal metabolic processes. Such advancements represent a transformation from density-based approaches towards the multidimensional system for understanding bone fragility used to assess fracture risk, track treatment outcomes and study the genetic mechanisms behind complex conditions like diabetic bone disease and glucocorticoid-induced osteoporosis. (5–8)

*Author for Correspondence: : Mr. Pratap Singh

The review provides a comprehensive overview of current quantitative imaging techniques used in osteoporosis assessment, highlighting their fundamental principles, clinical uses, technical advantages, disadvantages and their emerging role in personalized medicine systems.

1. Conventional Radiographic Assessment

1.1. Role of Plain Radiography in Osteoporosis Detection

Plain radiography is the most commonly used initial imaging technique in clinical practice and has long been the foundation for detecting reduced bone density and fragility fractures. However, it has an important challenge, as visible changes on radiographs appear only after about 30–50% of bone mineral has been lost, making it unsuitable for early detection of osteoporosis. Older techniques, such as radiogrammetry and radiographic absorptiometry, provides more objective estimate of bone mineral density (BMD), but these have now largely been replaced by advanced quantitative imaging techniques. Despite its limitations, plain radiography continues to be useful for detecting fractures, particularly in settings where DXA and QCT are not available. (7,9)

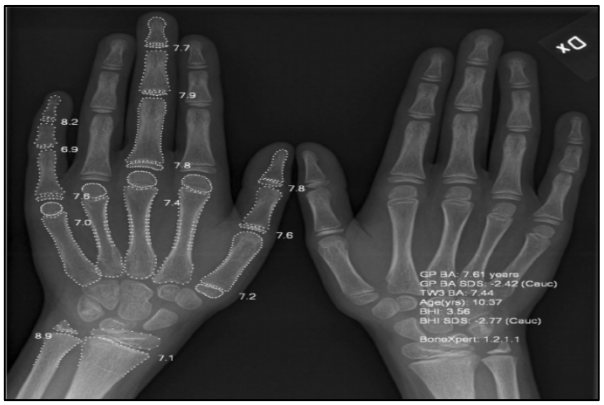

Figure 1: X-ray radiogrammetry of both hands of a patient with a Digital X-ray unit. Post-processing was performed using automated determination of bone age. (10)

1.2. Radiographic Features of Osteopenia and Fragility Fractures

Osteopenia exhibits its radiographic characteristics through three main features: increased radiolucency, loss of cortical bone, and heightened visibility of primary vertical trabecular patterns due to preferential loss of secondary horizontal trabecular structures. In the spine, alterations present as translucent vertebral bodies, forward-projecting endplates, and vertical striped patterns. The common spinal deformities comprise the biconcave “cod-fish” vertebra, the anterior wedge deformity, and the crush fractures.

The most important vertebral body, proximal femur, and distal radius fragility fracture results are clinically significant, while chest and spine radiographs show vertebral compression fractures as incidental findings during examinations for different medical conditions. The distinction between osteoporotic and malignant fractures becomes difficult when using plain films, leading to MRI evaluation when the diagnosis remains uncertain. (7,9)

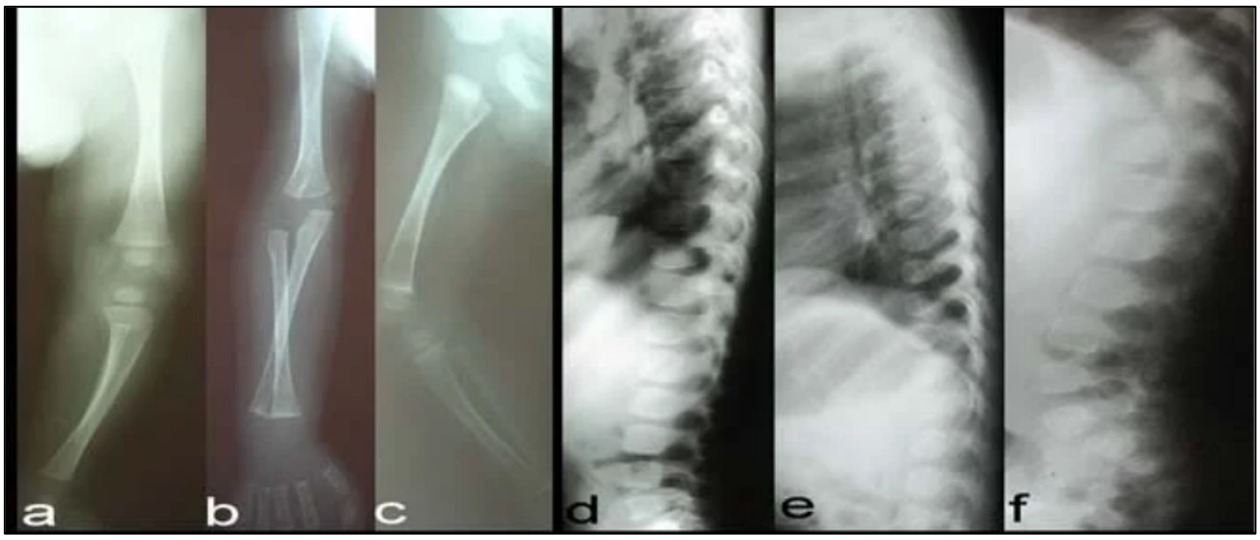

Figure 2: Interpretation of osteopenia in long bones using radiograph; patient 1 at the age of 2 months (a), patient at the age of 4 months (b), patient at the age of 8 months (c). Mild platyspondyly in a patient at the age of 2 months (d), patient having round vertebral bodies at the age of 4 months I, patient having mild platyspondyly at the age of 8 months (f). (11)

1.3. Vertebral Fracture Assessment and the Transition to Quantitative Methods

The limitations of plain radiography in systematically grading vertebral fractures led to the development of the Genant classification, which scores vertebral deformity by degree of height reduction. This framework directly laid the conceptual groundwork for vertebral fracture assessment (VFA), a lateral spine imaging technique performed on modern DXA platforms that enables systematic vertebral evaluation with low radiation exposure and is discussed further in the DXA section.(9–11)

Table: Genant classification of vertebral deformity based on percentage reduction in vertebral height.

Grade	Severity	Height Reduction	Description of Deformity
Grade 0	Normal	< 20%	No significant deformity
Grade 1	Mild	20–25%	Slight reduction in vertebral height
Grade 2	Moderate	25–40%	Noticeable reduction with clear deformity
Grade 3	Severe	> 40%	Marked collapse and significant deformity

1.4. Strengths and Diagnostic Limitations

The main advantages of plain radiography are its minimal cost, availability and ability to provide rapid image acquisition, essential in detecting fractures, assessing bone structure and identifying additional skeletal disorders. However, it has specific diagnostic limitations. Density assessment relies on qualitative evaluation that varies between different observers while being affected by technical parameters and body composition. In addition, radiography only provides a two-dimensional image, limiting the evaluation of volumetric BMD, bone microarchitecture, and changes that occur between cortical and trabecular bone.

Incidental vertebral fractures are often detected on chest or abdominal radiographs for non-related clinical indications, leading to missed opportunities for the early diagnosis of osteoporosis that requires further evaluation. Therefore, plain radiography serves as a diagnostic tool that supports quantitative imaging techniques. When combined with BMD values obtained through DXA, QCT, and HR-pQCT, it contributes to a comprehensive assessment of fracture risk. (7,9,12,13)

2. Dual-Energy X-Ray Absorptiometry (DXA)

Dual-energy X-ray absorptiometry (DXA) has been the clinical gold standard for bone densitometry for several decades, and remains the most widely used method to identify osteoporosis and determine fracture risk.(14–17) It establishes its central role in clinical practice through its ability to provide accurate BMD measurements from

essential skeletal sites while producing minimal radiation exposure, approximately 1 to 10 μSv, rapid scan times, and well – established normative reference databases. (18,19)

Despite the advantages, the development of imaging techniques has highlighted the inherent limitations of existing imaging systems, discussed further.

2.1. Physical Principles and Instrumentation

Dual energy X-ray absorptiometry (DXA) works on the measurement of X-ray attenuation at two photon wavelengths to differentiate between bone mineral content composed of hydroxyapatite and surrounding soft tissue. This results in the calculation of areal bone mineral density (aBMD), expressed in grams per square centimetre.

The technique is based on a two-dimensional projection system, which calculates aBMD by dividing mineral content by projected bone area. Therefore, this results in a measurement that shows sensitivity to bone size, while also exhibiting susceptibility to degenerative changes, which can lead to measurement errors.

Modern DXA technology primarily operates through fan beam systems. However, differences in beam geometry between major manufacturers, such as Hologic and GE Lunar, require cross-calibration to ensure consistency. In addition, routine daily phantom calibration is required to maintain measurement accuracy over time. (15,16,19,20)

2.2. Measurement Sites and Standardized Protocols

According to the World Health Organization (WHO) and the International Society for Clinical Densitometry (ISCD), DXA measurements should begin at three primary sites:

- Posteroanterior (PA) lumbar spine (L1–L4)
- Proximal femur (total hip and femoral neck)
- Distal one-third radius measurements

The forearm site is mainly useful when spine and hip measurements are not achievable or in conditions such as primary hyperparathyroidism. (16,19,21,22)

The WHO classification mainly relies on femoral neck measurements for the diagnosis of osteoporosis. The lumbar spine, consisting of a higher proportion of trabecular bone, is more sensitive to changes and therefore utilized for monitoring the treatment responses than other sites.

In pediatric populations, the ISCD recommends assessment of total body less head (TBLH) and PA spine measurements, with results reported as Z-scores. Accurate DXA assessment requires standardized patient positioning along with consistent ROI placement and serial measurements. When different DXA systems are used, cross-calibration between platforms is necessary to ensure reliable comparisons.(17,21,23,24)

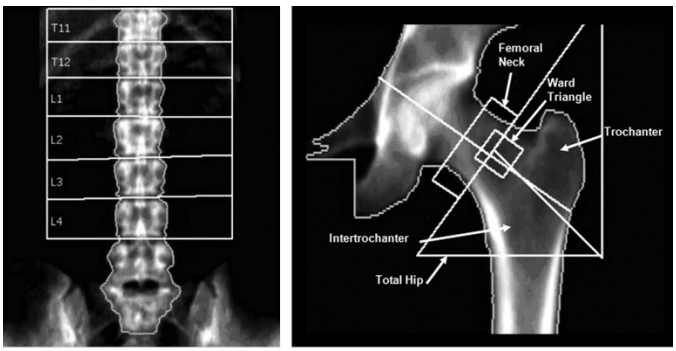

Figure 3: Standard DXA measurement sites and region-of-interest (ROI) placement: (A) posterior-anterior lumbar spine (L1–L4), (B) proximal femur (femoral neck and total hip) (25)

2.3. T-Score, Z-Score, and WHO Diagnostic Criteria

DXA-derived bone mineral density (BMD) is interpreted using the T-score and Z-score methods through comparison with reference populations. The WHO classification applicable to postmenopausal women and men aged 50 years and older defines four T-score categories given below. The WHO also identifies the femoral neck T-score as both their diagnostic reference standard and an essential FRAX® tool.

Table: WHO classification of osteoporosis based on T-score with clinical application of T-score and Z-score.

Category	T-score Range	Clinical Interpretation
Normal	≥ −1.0	Normal bone density
Osteopenia	−1.0 to −2.5	Low bone mass
Osteoporosis	≤ −2.5	Increased fracture risk
Severe Osteoporosis	≤ −2.5 + fragility fracture	Advanced disease with fractures

Z-scores are preferred in premenopausal women, men under 50 years of age, and children with values ≤−2.0 defined as below the expected range for age. However, a large percentage of fragility fractures occur in individuals with osteopenic T-scores, highlighting the limitations of relying on BMD-based fracture risk assessment methods. (17,26–28)

2.4. Precision, Accuracy, and Longitudinal Monitoring

DXA measurements demonstrate a 1–2% precision for lumbar spine assessments and 1.5–2.5% precision for proximal femur assessments when performed under controlled conditions. The least significant change (LSC), typically 0.03–0.05 g/cm² at the femoral neck, defines the minimum change interpretable as biologically meaningful at a 95% confidence level.

However, the projection nature of DXA introduces certain limitations. Areal BMD (aBMD) consistently shows lower BMD results for smaller individuals while producing higher BMD results for larger individuals. In addition, the presence of osteophytes, endplate sclerosis, and aortic calcification in degenerative lumbar changes results in false BMD elevation, leading to misinterpretation.

ISCD recommends that all serial measurements be performed using the same device and software version. If a change is unavoidable, formal cross-calibration is required to ensure accurate comparison. (15,19,23)

2.5. Advanced DXA Applications

Advanced DXA techniques develop assessment beyond bone mineral density by evaluating bone quality, vertebral integrity, body composition, and structural strength, improving fracture risk stratification.

Table: Advanced DXA applications for comprehensive skeletal and body composition assessment.

Application	Principle / Measurement	Clinical Utility	Advantages	Limitations	Reference
Trabecular Bone Score (TBS)	Lumbar spine texture analysis reflecting trabecular microarchitecture	Enhances fracture risk prediction (FRAX®); useful when BMD is misleading (e.g., diabetes, glucocorticoid use)	Complements BMD	Affected by BMI and soft tissue thickness	(17,19,29)
Vertebral Fracture Assessment (VFA)	Lateral spine DXA imaging (T4–L4)	Detects and grades vertebral fractures; influences management decisions	Low radiation; detects occult fractures	Lower image resolution	(19)

Body Composition Analysis	Whole-body DXA for lean and fat mass distribution	Evaluates sarcopenia and osteosarcopenia	Quantitative and reproducible	Limited standardized athletic references	(19,23)
Hip structural analysis (I) **Bone Strain Index (BSI)**	Geometric and biomechanical analysis of the proximal femur	Assesses bone strength and resistance to stress	Provides structural insight beyond BMD	Model-based; limited routine use	(19)

2.6. Limitations and Sources of Error

DXA has several important limitations, including its inability to differentiate between cortical and trabecular bone compartments. Its accuracy is reduced in patients with orthopedic implants, severe scoliosis or extreme body habits. In addition, the incomplete validation of pediatric normative reference data across all demographic groups represents its most serious limitations. (15,20)

To address these limitations, several advanced quantitative imaging techniques have been developed, which are discussed in the following sections. These approaches provide complementary information and enhance the overall assessment of bone health when used along with DXA. (24)

3. Quantitative Ultrasound (QUS)

Quantitative ultrasound (QUS) is a non-ionizing technique that analyzes bone properties by evaluating its density, elasticity, microarchitecture, and strength. It functions as an additional tool that detects bone quality elements that are not captured by the areal BMD measurements of DXA. In addition, it serves as an essential pre-screening instrument in regions with limited DXA access.

QUS transmits pulsed ultrasound waves through bone material to produce two main outputs depending on the trabecular microstructure and porosity.

- Speed of sound (SOS), indicating trabecular stiffness and interconnectivity
- Broadband ultrasound attenuation (BUA), measuring frequency-dependent energy loss

Ex vivo calcaneal research demonstrates that SOS measurement directly relates to bone density, trabecular thickness, bone volume fraction, and compressive strength, with the relationship remaining intact after BMD correction. In contrast, BUA detection exhibits high sensitivity to plate-to-rod trabecular transformations, which occur during the initial stage of remodelling disruption.

This dual sensitivity enables its function as a significant fracture risk predictor, applying to non-spinal locations where structural damage happens before density reduction occurs. (30–32)

3.1. Quantitative Ultrasound (QUS) Parameters and Clinical Correlation

The fundamental QUS parameters include: Speed of Sound (SOS) and Broadband Ultrasound Attenuation (BUA), and composite indices show bone density and trabecular structure information. The parameters show a moderate to strong relationship with DXA-derived measurements, assisting in estimating fracture risk.

Table: QUS parameters, their ranges, and correlation with bone density and fracture risk (30–33)

Parameter	Typical Range / Value	Correlation / Relationship	Clinical Significance
Speed of Sound (SOS)	1,600–1,700 m/s	Correlates with DXA femoral neck T-score (r = 0.65–0.80)	Reflects bone density and elasticity; minimally affected by hydration

Broadband Ultrasound Attenuation (BUA)	40–120 dB/MHz	Inversely correlates with bone volume fraction (r = −0.55 to −0.75)	Sensitive to trabecular structure and plate loss
Composite Indices (e.g., Stiffness Index, QUI)	Derived from SOS & BUA	Predict fracture risk (hazard ratio 1.4–2.2 per SD decline)	Comparable to DXA for fracture risk prediction in large studies

3.2. Peripheral Measurement Sites

QUS measurement primarily occurs at the calcaneus because its high trabecular density and optimal technical properties enable precise fracture risk evaluation. The measurement process needs population-specific reference standards to interpret results, yet remains clinically useful through additional peripheral testing sites and established measurement techniques. (31,33,34)

Table: Essential QUS measurement parameters and site-specific data.

Parameter	**Key Data**
Primary Site (Calcaneus)	>90% usage; ~95% trabecular bone
Precision (Calcaneus)	SOS: CV 0.4–1.2% BUA: CV 1.8–3.5%
Fracture Risk (Calcaneus)	Hip fracture HR ~1.7 per SD decline
Other Sites	Mid-tibia (cortical), distal radius (cancellous), phalanges (HR ~1.3)
Techniques	Through-transmission; pulse-echo
Population Variation	South Asians differ by ~0.3–0.5 SD from the Caucasian reference

3.3. Clinical Applications in Screening and Risk Prediction

In primary care, QUS has seen a reduction in DXA requests by 40-60% while maintaining accuracy of 82-92% for identification of DXA T-scores ≤−2.0 in postmenopausal women, leading to affordable patient evaluation. Studies have also established that SOS and BUA could predict fractures with hazard ratios that ranged from 1.5 to 2.0 for non-spine fractures and 1.3 to 1.7 for hip fractures per drop in the standard deviation.

In addition, QUS parameters with FRAX improve the predictive parameters, increasing approximately 0.68 to 0.72 – 0.81 with area under the curve (AUC). When incorporated with machine learning, AUC further improves by approximately 0.85, while further validation is necessary. (35–37)

Regional studies in the South Asian population, including India, demonstrate QUS as an effective tool for locating cases in locations without DXA facilities, with a correlation range of r = 0.62–0.78. QUS is also useful in detecting increased fracture risk in individuals on glucocorticoid therapy and type 2 diabetes mellitus, exhibiting ~1.8 times higher risk than the general population

In pediatric populations, age-specific reference data support the use of QUS for monitoring peak bone mass development. Guidelines from organizations such as the National Osteoporosis Foundation (NOF) and the International Osteoporosis Foundation (IOF) include combined approaches such as hybrid QUS-FRAX and QUS-DXA algorithms as a standard assessment strategy. (37,38)

3.4. Advantages and Technical Constraints

QUS presents as an emerging modality in bone health assessment, offering a non-ionizing, cost-effective, and portable alternative for evaluating skeletal integrity beyond conventional BMD measurements, given below:

Advantages of QUS

- **Non-ionizing technique** – safe for repeated use without radiation exposure

- **Portable equipment** – devices can weigh less than 2 kg, suitable for field and rural use
- **Cost-effective** – relatively affordable (approximately $3,000–$25,000)
- **Rapid results** – scan time is usually within 60 seconds
- **Easy to operate** – requires minimal operator training
- **Broad applicability** – can be used in patients with implants or extreme body habitus without major restrictions

Limitations of QUS

- **Lower precision than DXA** – coefficient of variation ranges from 0.8% to 5% (vs. 0.8%–2% in DXA)
- **Inter-device variability** – T-score differences of 0.7–1.2 SD between manufacturers
- **Limited monitoring capability** – less sensitive to small treatment-related BMD changes (1–3% annually) compared to DXA (2–6%)
- **Temperature sensitivity** – SOS measurements decrease by ~1–2% per °C increase (though modern devices apply correction algorithms)

Clinical Recommendation: According to the International Society for Clinical Densitometry and the International Osteoporosis Foundation, QUS is recommended for screening and risk stratification; DXA confirmation is required before initiating treatment. (31,37,38)

4. Quantitative Computed Tomography (QCT)

4.1. Technical Principles and Calibration Techniques

QCT uses phantom-based calibration to transform Hounsfield unit (HU) data into volumetric BMD (vBMD, mg/cm³), delivering accurate three-dimensional density measurements. It remains unaffected by bone size, soft tissue and degenerative changes, providing a fundamental benefit over DXA two-dimensional areal measurements. It also enables vBMD estimation from existing clinical CT datasets, which were obtained for different purposes when phantom scanning cannot occur at the same time. (12,13,39,40)

4.2. Volumetric BMD and Trabecular–Cortical Differentiation

The primary clinical advantage of QCT lies in its ability to measure cortical bone and trabecular bone areas as separate entities. At sites such as the lumbar spine and proximal femur, trabecular vBMD detects initial bone loss and treatment effects better than DXA aBMD.

In addition, QCT provides information on bone structure, measuring bone geometry and cortical thickness, serving as important factors that determine bone strength. Advanced applications, such as the QCT-based finite element analysis (FEA) extension transforms voxel-level density data into a biomechanical model estimating bone stiffness and failure load for assessing fracture resistance of vertebral and femoral bones. (40–42)

4.3. Peripheral QCT (pQCT) and High-Resolution pQCT (HR-pQCT)

Peripheral quantitative computed tomography (pQCT) is used to measure the bone density and geometry of the distal radius and tibia. It involves lower radiation exposure than central QCT to produce specific volumetric BMD (vBMD) and geometric measurements, including cortical thickness and cross-sectional moment of inertia.

The HR-pQCT system, with systems such as XtremeCT I with a resolution of 82 μm and XtremeCT II with a resolution of approximately 61 μm, enables complete microarchitectural assessment. It allows measurement of trabecular number, thickness, separation and bone volume fraction with cortical thickness and porosity, which DXA and standard QCT cannot detect. In addition, micro-finite element analysis (μFEA) applied to HR-pQCT datasets yields estimates of bone stiffness and failure load. The meta-analysis conducted by Cheung et al. (2020) demonstrated that HR-pQCT parameters, particularly cortical vBMD and trabecular thickness, can independently assess fracture risk beyond DXA limits, with the distal radius and tibia conducting complementary predictive assessments. (43–45)

HR-pQCT has been incorporated into major studies such as MrOS, OFELY, CaMos and the Framingham Osteoporosis Study. These studies describe changes in microarchitectural structure based on menopausal status,

fracture history, and metabolic bone disease, as well as treatment response through structural changes measured following antiresorptive and anabolic therapies.

Despite advanced diagnostic capabilities, clinical adoption remains limited. This is due to limited facilities worldwide, high cost, motion artifacts affecting diagnostic accuracy, and a lack of validated normative databases across multiple population groups. Current priorities for image analysis pipelines include standard procedures and validating HR-pQCT through micro-CT examination, serving as the histological reference standard. (46–48)

4.4. Opportunistic Osteoporosis Screening Using Routine CT

Opportunistic CT screening uses routine CT scans obtained for different medical purposes. These scans include abdominal, chest and pelvic studies. It enables the detection of individuals at increased risk of fractures without exposing them to any additional radiation.

The Density measurement for vertebral trabecular ROIs can be determined through two methods.

- The first method uses HU measurement of vertebral trabecular ROIs
- The second method uses phantom-calibrated or asynchronous calibration, which converts HU to vBMD equivalents.

Advances in AI have further enhanced this approach. Automated AI algorithms allow to perform vertebral segmentation, BMD estimation and fracture detection with equal effectiveness to dedicated QCT systems. These methods are typically validated using large retrospective datasets. (13,49)

Emerging technologies continue to increase the capabilities of CT-based bone assessment. Dual-energy CT (DECT) enables material decomposition of calcium and soft tissue, allowing BMD estimation and bone marrow characterization without a calibration phantom. Photon-counting CT (PCCT) offers superior spatial resolution, reduced electronic noise, and intrinsic spectral information, properties that may further enhance microarchitectural detail and opportunistic BMD quantification in future clinical workflows. (12,13)

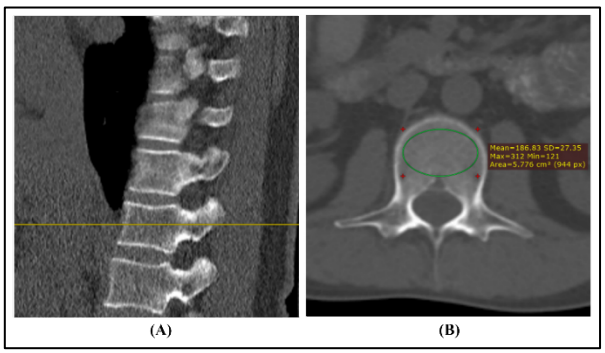

Figure 4: Opportunistic diagnosis of osteoporosis during abdominal CT: (A) Selection of axial image passing from the center of vertebrae, and (B) placement of ROI at axial image to measure mean HU. (50)

4.5. Radiation Dose and Clinical Considerations

Central QCT involves an effective radiation dose that ranges between 0.25 and 1 mSv, higher than the radiation dose from DXA (ranges from 0.001 to 0.01 mSv) but falls within the range of most standard diagnostic CT scans. Modern low-dose protocols for CT scanning with iterative reconstruction methods have enabled a continuous decline in effective radiation dose.

In comparison, HR-pQCT delivers only ~5 μSv per scanned centimetre, well below a standard chest radiograph (~50–70 μSv), making it particularly suitable for follow-up studies and use in younger populations.

Several technical factors, such as CT scanner type, reconstruction kernel, tube voltage and slice thickness, affect the HU values determining the vBMD results. Therefore, cross-scanner standardization is essential to ensure precise consistency and accuracy.

The main challenge faced is the lack of universally accepted HU-based diagnostic thresholds established for opportunistic osteoporosis screening. Organizations such as the International Society for Clinical Densitometry (ISCD) are working towards their consensus development process. (43,44,46)

5. Magnetic Resonance Imaging (MRI)

Magnetic resonance imaging (MRI) provides non-ionizing, multi-parametric assessment of bone marrow composition, trabecular and cortical microarchitecture, and metabolic activity, dimensions inaccessible to DXA or standard QCT.(51,52) The advanced technology enables faster imaging and better AI performance, expanding its role in research and clinical settings for the evaluation of osteoporosis.

MRI utilizes differences in proton density, T1 and T2 relaxation times, and magnetic susceptibility to characterize bone marrow composition at spatial resolutions of 100–400 μm on 3T and 7T systems. The bone marrow fat fraction (BMFF) shows an increase in osteoporosis, with adult vertebral BMFF ranging from 25% to 80%. This highlights a shift in mesenchymal stem cells that differentiate into fat cells instead of bone-building cells. BMFF inversely correlates with lumbar BMD ($r = -0.52$ to -0.75) and trabecular BV/TV ($r = -0.60$ to -0.82). (53–55)

High-resolution structural MRI techniques, such as multi-echo gradient echo (ME-GRE) and susceptibility-weighted imaging (SWI) provides three-dimensional analysis of trabecular microarchitecture by measuring trabecular thickness, separation, number, and connectivity density and plate-to-rod ratio, which identify strong connections to elastic modulus measurements ($r = 0.85–0.96$) and can predict bone fracture risk independently. (53,55,56)

Advanced MRI sequences, including ultrashort echo time (UTE) and zero echo time (ZTE), enable detection of cortical bone signals from bound water protons at the collagen-mineral interface and pore water within Haversian canals. It serves as indicators of bone structure integrity and osteolytic bone loss. However, these tools remain exclusive to specialized research applications on advanced high-field imaging systems. (53,56)

5.1. Quantitative MRI Techniques: Relaxometry, Diffusion, and Dixon Methods

Relaxometry methods include T1 mapping (sensitive to marrow hypocellularity, with T1 prolongation of ~15–30% in osteoporosis), T1ρ imaging (sensitive to collagen cross-link integrity and proteoglycan content), and T2* mapping — where R2* (= 1/T2*) scales inversely with BV/TV ($r = -0.68$ to -0.88) and correlates with ex vivo vertebral stiffness, providing an indirect microstructural index derivable from standard clinical MRI hardware. (51,52,57)

Diffusion tensor imaging (DTI) yields ADC, fractional anisotropy, and mean diffusivity from bone marrow; ADC is elevated ~25–45% in osteoporotic marrow reflecting reduced cellular packing, though DTI tractography is not yet clinically validated for osteoporosis. Multi-echo Dixon PDFF quantification enables breath-hold volumetric fat mapping of the spine and proximal femur (CV <1.2%) with demonstrated sensitivity to treatment effects: bisphosphonate therapy reduces BMFF by ~7–18%, while aromatase inhibitor use increases it by ~10–22%.

Relaxation- based MRI techniques provide additional information on bone quality. T1 mapping can detect marrow hypocellularity, with T1 values that increase by approximately 15 to 30% in osteoporosis cases. T1ρ imaging detects collagen cross-link integrity and proteoglycan content. T2* mapping shows that R2*, which equals 1 divided by T2*, displays an inverse relationship with BV/TV according to the range of r values, extending from -0.68 to -0.88. The relationship between R2* and vertebral stiffness establishes a pathway to determine microstructural characteristics through standard clinical MRI equipment. (58)

Diffusion tensor imaging (DTI) includes three parameters: apparent diffusion coefficient (ADC), fractional anisotropy, and mean diffusivity within bone marrow. In osteoporotic marrow, ADC value increases by approximately 25 to 45% due to decreased cellular density. Although DTI tractography requires clinical validation to assess osteoporosis cases.

The multi-echo Dixon technique allows quantification of proton density fat fraction (PDFF), enabling spine and proximal femur fat volume measurement. It typically requires breath-holding while achieving volumetric fat

measurement to prove treatment effects at a coefficient of variation below 1.2%. The bisphosphonate therapy decreases bone marrow fat fraction by approximately 7 to 18%, while the aromatase inhibitor results in a bone marrow fat fraction increase of approximately 10 to 22%. (59)

5.2. Trabecular Microarchitecture and Cortical Porosity Analysis

High-field MRI (3T and 7T) enables individual trabecula segmentation and topological analysis, which distinguishes between plate-like and rod-like elements. Postmenopausal women experience a ~30% reduction in plate volume fraction, and the plate-to-rod dissociation index shows strong correlation with μFE-based failure load measurements, having a correlation range of r = 0.82–0.94.

Bi-exponential T2* fitting and IR-UTE sequences enable measurement of cortical porosity ranging from 3% to 30% across different skeletal sites. Every 10% increase in measurement raises hip fracture risk by 2.8 to 3.5 times, while denosumab treatment leads to cortical porosity reduction of approximately 12% to 20% through RANKL blockade. (53,55,56)

5.3. MR Spectroscopy and Fat Fraction Quantification

Single-voxel ^{1}H-MR spectroscopy (SVS) provides highly accurate measurements of bone marrow fat fraction (BMFF) with a coefficient of variation between 1.8 and 3.5%. It also enables assessment of lipid unsaturation levels, showing a reduction between 15 and 25% due to osteoporosis.

Multi-peak Dixon-based proton density fat fraction (PDFF) shows excellent agreement with single-voxel spectroscopy (r = 0.94–0.99) while offering whole-skeleton volumetric coverage in 8–12 minutes, making them more practical option for routine research protocols.

These techniques show sensitivity to treatment-related changes. Anabolic therapies such as romosozumab and teriparatide reduce BMFF by approximately 10 to 20% while increasing trabecular thickness by about 15 to 25%. In contrast, antiresorptive therapy with alendronate decreases the lipid saturation index by approximately 8%.

Three-dimensional chemical shift imaging (3D-MRSI) allows assessment of multiple vertebral levels at the same time, while its reduction of olefinic signal indicates increased risk for vertebral fracture development, which has a hazard ratio of 2.3. More advanced techniques, such as phosphorus (^{31}P) and carbon (^{13}C) spectroscopy prevents its use in routine clinicals. (54,59)

5.4. Clinical and Research Applications

MRI plays a key clinical role in the identification of vertebral compression fractures, particularly in differentiating acute and chronic fractures. This is achieved through identification of marrow edema using STIR or fat-suppressed T2- weighted sequences. It also plays an important role in the oncologic assessment of bone, helping differentiate osteoporotic fractures from malignant involvement and guiding appropriate treatment decisions.

Beyond fracture detection, Multi-parametric MRI provides advanced fracture risk assessment and disease subtype classification. These include glucocorticoid-induced marrow adiposity, type 2 diabetes–related dissociation between marrow fat and BMD, and hyperparathyroidism-associated cortical porosity. It also provides non-invasive resources to monitor drug effects in both clinical and research settings. (51,52,54)

Recent advances in AI methods have enhanced MRI techniques. Convolutional neural networks model receives training on both MRI and μFE data to accomplish fracture prediction through AUC 0.90–0.96, demonstrating better results than DXA alone, with its 0.72 prediction accuracy. In addition, hybrid approaches such as MRI-QCT and MRI-radiomics pipelines provide accurate skeletal phenotype identification.

Despite these advantages, the practical limitations restrict its clinical use. These include high scan costs and long acquisition time (20–50 minutes), motion artifact vulnerability and field inhomogeneity in obesity or kyphosis conditions. However, the clinical feasibility of accelerated protocols that combine IDEAL-PDFF and T2* mapping and diffusion imaging within 12–18 minutes has improved through cloud-based AI postprocessing. (51,53,55)

6. Positron Emission Tomography (PET)

6.1. Molecular Imaging of Bone Metabolism

The ^{18}F-sodium fluoride (^{18}F-NaF) PET method represents the most advanced technique for detecting bone metabolism through molecular imaging, enabling measurement of bone turnover rates by observing bone blood circulation and ongoing hydroxyapatite surface changes. ^{18}F-fluoride ions incorporate at sites of active remodelling, serving as a regional proxy for bone formation rate, though uptake reflects surface turnover and perfusion rather than osteoblast number directly. (60,61)

The ^{18}F-NaF method achieves three times greater bone distribution than traditional ^{99m}Tc-MDP bone scintigraphy while delivering superior image resolution and quantitative accuracy, making it an essential research instrument for studying bone physiology and pathology. (62–64)

6.2. ^{18}F-NaF PET for Bone Turnover Evaluation

Static SUV measurements and dynamic Patlak kinetic modelling are the two methods used in ^{18}F-NaF PET analysis to determine the net fluoride influx constant (Ki), which serves as a more accurate biological measurement of bone formation rate that remains unaffected by changes in blood flow.(65) ^{18}F-NaF PET provides better sensitivity and spatial resolution than planar scintigraphy and SPECT, which allows to highlight the metabolic abnormalities in osteoporosis studies and cancer-related bone disease research.(66,67)

6.3. Hybrid Imaging: PET/CT and PET/MRI

The combination of PET and CT technology enables the use of metabolic activity maps and structural CT data with attenuation correction. It identifies active bone turnover regions while studying local structural alterations that include cortical thinning and trabecular disruption. It also distinguishes between bone metastases that show metabolic activity and bone degeneration caused by simultaneous osteoporosis and cancer presence. (68)

PET/MRI substitutes the CT part with simultaneous MRI acquisition, which provides better soft tissue imaging and bone marrow assessment without exposing patients to CT radiation. It makes it especially beneficial for children and individuals with detailed imaging of marrow infiltration or edema. This is due to conditions that require precise visual assessment of affected areas. It integrates ^{18}F-NaF metabolic assessment with MRI multi-parametric marrow evaluation to establish a thorough skeletal phenotyping system. (69,70)

6.4. Role in Osteoporosis Research and Treatment Monitoring

The ^{18}F-NaF PET imaging technique has proven its value as a research tool for osteoporosis studies. It detects changes in bone metabolism before DXA measurements show BMD changes. Therefore, useful for assessing the effects of antiresorptive and anabolic treatments according to their Ki values from Patlak modelling, serving as initial clinical trial results. (71)

The evidence base in primary osteoporosis remains limited compared to data from oncological studies due to most published research focusing on metastatic bone disease, Paget's disease and other conditions that exhibit high bone turnover. Clinicians interpreting serial scans must anticipate the flare phenomenon, a transient uptake increase after effective therapy that reflects reactive bone remodelling, not progression.(72,73) The newly developed tracers ^{68}Ga-labeled bisphosphonate analogues and agents that target RANKL and sclerostin pathways may provide better techniques to assess bone activities between osteoblasts and osteoclasts.(71)

6.5. Practical Limitations and Clinical Feasibility

The practical limitations restrict the routine ^{18}F-NaF PET application for osteoporosis diagnosis stem from its high price, unpredictable insurance coverage, and requirement for cyclotron access, which supports the tracer's 110-minute half-life.(74,75)

The challenge of diagnosing osteoporotic individuals through bone scans arises due to their elevated uptake pattern, which appears in both healthy bone healing and various medical conditions, along with cancerous tumors. The effective radiation dosage from ^{18}F-NaF PET examination depends on 4 to 7 mSv, which increases to 5 to 8 mSv when the CT component of the PET/CT scan is added; PET/MRI systems maintain the same tracer dosage without exposing patients to CT radiation.(76)

7. Comparative Evaluation of Quantitative Imaging Modalities

The complete assessment of skeletal weakness requires multiple techniques, as no single method can provide all necessary information. The table below summarises key performance domains, radiation burden, cost and accessibility, microarchitectural capability, fracture risk prediction, longitudinal suitability, and primary application across the seven modalities reviewed. The clinical deployment of each technique is shaped by the specific question being addressed: DXA anchors diagnosis and monitoring; QCT and opportunistic CT extend quantitative BMD assessment; HR-pQCT and MRI serve research phenotyping; QUS enables low-resource triage; and PET provides unique molecular metabolic data.

The combination of sequential and multimodal strategies allows for testing, which starts with QUS triage and progresses to DXA testing while also enabling the use of DXA with TBS for microarchitectural analysis and DXA with VFA for vertebral fracture identification without needing advanced research facilities.

Table: Comparison of imaging modalities based on radiation, cost, structural assessment, and clinical utility.

Modality	**Radiation Exposure**	**Cost & Availability**	**Microarchitectural Assessment**	**Fracture Risk Prediction**	**Longitudinal Monitoring**	**Primary Application**
Plain Radiography (12,77)	Low	Widely available, very low cost	None (qualitative only)	Poor (insensitive to early loss)	Not applicable	Fracture detection
DXA (78–80)	Very low (1–10 µSv)	Widely available, moderate cost	None (2D areal BMD)	Excellent (validated T-score)	Excellent	Clinical standard
QCT (78,80,81)	Moderate (0.25–1 mSv)	Moderately available, higher cost	Good (3D, compartmental)	Good; excellent with FEA	Moderate	Clinical & research
HR-pQCT (44,81,82)	Very low (~3–5 µSv/site)	Very limited, very high cost	Excellent (in vivo microstructure)	Very good (incremental to DXA)	Good (research)	Research
QUS (77,79)	None	Widely available, very low cost	Indirect (SOS, BUA)	Moderate (comparable to DXA for hip)	Limited	Screening & triage
MRI (12,78)	None	Moderately available, high cost	Very good (marrow + microstructure)	Good (research cohorts)	Moderate (research)	Research
PET (^{18}F-NaF) (12,83)	High (4–15 mSv with CT)	Limited, very high cost	None (metabolic only)	Emerging	Limited	Research & oncology

8. Emerging Technologies and Artificial Intelligence

AI and advanced computational imaging are rapidly reshaping osteoporosis assessment, addressing limitations: underdiagnosis of vertebral fractures, insensitivity of BMD-based metrics to bone quality, and underutilization of CT data acquired for other clinical indications.

8.1. Machine Learning in Opportunistic CT-Based BMD Assessment

The complete BMD analysis process includes vertebral segmentation, trabecular ROI placement, and HU extraction with BMD equivalence conversion. This process can be fully automated by AI-based tools, enabling opportunistic CT without needing any radiologist manual work.

CNN models trained on large retrospective CT datasets demonstrate performance comparable to phantom-calibrated QCT across diverse scanner types and patient populations, with several tools receiving or pending regulatory clearance. The extensive global CT usage generates a major clinical effect, while two main obstacles remain, including the need for standard HU-based diagnostic thresholds and the requirement for prospective outcome research to show that opportunistic screening results in fracture prevention benefits, beyond its ability to enhance detection rates.(13,49)

8.2. Automated Vertebral Fracture Detection

Fewer than one-third of incidentally visible vertebral fractures are reported on routine radiological reads. Automated detection systems trained on CT and DXA-VFA images with Genant grading frameworks achieve sensitivity and specificity approaching or exceeding expert radiologist performance, while eliminating fatigue-related variability and standardizing reporting across institutions. (7,13)

Current limitations include variable performance on non-standard spinal anatomy such as scoliosis, post-surgical changes, severe degenerative disease, reduced sensitivity for Grade 1 deformities, and dataset characteristics that may not generalize across all ethnic populations or protocols; integration into radiology information systems with radiologist oversight is the pragmatic path to routine implementation.

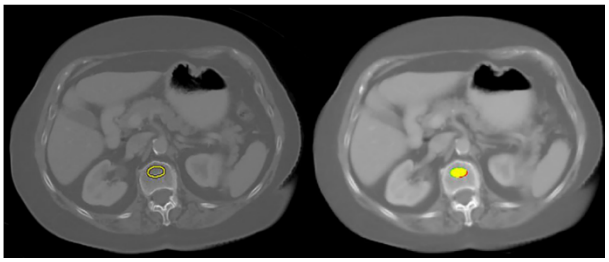

Figure 5: Comparison of manual and automated L1 trabecular ROI (Region of Interest) on abdominal CT scans in a 70-year-old woman. Left Image represent axial image showing a manually placed oval ROI in the L1 trabecular space. The right image shows an automated ROI region, having the older feature-based image processing algorithm (red-yellow) and the newer deep learning algorithm (green-yellow). The area of overlap is indicated by the yellow colour between the two automated methods.(84)

8.3. Radiomics and Texture-Based Bone Quality Analysis

Radiomics extracts high-throughput quantitative features (texture, shape, histogram metrics) from CT and MRI images of bone, capturing trabecular heterogeneity and cortical texture beyond mean HU values or BMD. Vertebral CT radiomic signatures have improved AUC for fracture prediction by 0.05–0.12 beyond DXA-based BMD in published cohort studies, particularly identifying structurally fragile individuals with osteopenic T-scores; MRI-based radiomics adds sensitivity to marrow compositional changes preceding gross density loss, and hybrid CT-MRI radiomic models are an active development area. (85–87)

Note that TBS, though sharing conceptual overlap with radiomics in its pixel-level gray-level variation approach, was developed independently within the DXA framework and should not be classified as a radiomic technique. The principal barrier to clinical translation is feature reproducibility: radiomic features are sensitive to scanner manufacturer, tube voltage, reconstruction kernel, and slice thickness; the Image Biomarker Standardization Initiative (IBSI) is working to harmonize feature definitions, but cross-institutional validation remains an ongoing priority. (85,86)

8.4. Broader AI Considerations: Explainability, Validation, and Clinical Integration

Several cross-cutting considerations apply across all three AI application domains. Many high-performing deep learning models operate as black boxes, raising concerns about accountability and regulatory approval; explainability methods such as Grad-CAM and SHAP are increasingly applied, but no consensus explainability standard for medical imaging AI currently exists. External validation across diverse populations, scanner types, and healthcare settings is essential before clinical deployment, yet many published studies report only internal validation metrics, and performance degradation on out-of-distribution data remains a well-documented vulnerability.

Federated learning, a collaborative model training across institutions without centralizing patient data, offers a promising solution to the tension between large, diverse training datasets and data privacy constraints; several consortia are actively developing federated osteoporosis AI initiatives. The regulatory landscape is evolving rapidly: multiple tools for opportunistic CT BMD assessment and vertebral fracture detection have received or are under FDA 510(k)/CE review, marking a transition from research tools to regulated medical devices; clinicians should verify regulatory status and post-market surveillance obligations before adoption. (86)

9. Challenges and Future Directions

Despite remarkable advances across quantitative imaging modalities for osteoporosis, significant challenges remain before these technologies can deliver their full clinical and public health potential.

9.1. Standardization and Reproducibility

Cross-platform standardization remains one of the most persistent challenges in quantitative bone imaging. For DXA, differences in calibration, edge detection, and manufacturer-specific reference databases introduce systematic BMD discrepancies affecting diagnostic classification. For CT-based methods, variability in scanner hardware, tube voltage, reconstruction kernels, and slice thickness produces substantial HU measurement variability, an acute issue in opportunistic CT screening, where scanner heterogeneity is inevitable (19,23,26)

QIBA has developed standardized CT-based BMD protocols representing an important step toward harmonization; Dixon-based PDFF quantification has demonstrated exceptional MRI reproducibility across field strengths and manufacturers, setting a methodological reference point for quantitative MRI biomarker development. (88,89)

9.2. Development of Reference Databases

The diagnostic utility of any quantitative imaging modality depends on robust, population-representative normative reference databases, yet significant gaps persist for pediatric populations, male patients, and non-European ethnic backgrounds.(24) The clinical consequences are real: a study of Mexican pediatric populations demonstrated vBMD values ~40% lower than Caucasian norms, risking systematic misclassification; the China Kadoorie Biobank generated vBMD normative data from opportunistic CT in over 69,000 adults, revealing significant geographic variation in osteoporosis prevalence within a single country. (26)

Reference data are even more limited for newer modalities: HR-pQCT normative databases remain largely derived from European and North American cohorts, while MRI-based biomarkers lack standardized reference ranges for routine clinical use across most populations. Developing ethnically and geographically diverse normative datasets is a research priority across all modalities.(90)

9.3. Regulatory and Clinical Adoption Barriers

DXA holds a recognized regulatory-approved position for osteoporosis diagnosis. Several newer modalities, including QCT, HR-pQCT, MRI-based bone biomarkers, and REMS, have not yet received uniform endorsement across jurisdictions, limiting their use to research or supplementary clinical roles.(17,91) REMS (Radiofrequency Echographic Multi-Spectrometry) is a non-ionizing, ultrasound-based technology that analyzes radiofrequency signals from bone; Zambito et al. (2025) report sensitivity and specificity exceeding 90% in selected cohorts, approaching quality-assured DXA performance, but REMS lacks ISCD review and standardized protocols and should be considered emerging rather than established. (91)

For AI-based tools, the regulatory environment is evolving rapidly: several tools for opportunistic CT BMD assessment and vertebral fracture detection have received FDA 510(k)/CE clearance, but ongoing scrutiny regarding post-market surveillance, model drift, and demographic subgroup performance means published AUC values (0.90–0.97) from single-institution internal validation sets do not reliably predict real-world performance. (18,92)

9.4. Need for Large-Scale Validation Studies

Most imaging biomarkers and AI-driven approaches reviewed here lack the large-scale prospective multicentre validation needed for guideline incorporation. Two gaps are critical:

- Clinical outcome linkage, demonstrating that a biomarker-driven screening pathway leads to measurable fracture incidence reduction, not merely improved detection (the China Kadoorie Biobank showed opportunistic CT screening is operationally feasible, but prospective fracture-prevention data are absent) (26)
- External generalizability, AI and radiomic models trained on specific datasets frequently degrade when applied to external populations, different scanner types, or non-standard protocols; deep learning classifiers for osteoporosis screening from chest radiographs are particularly vulnerable to overfitting; similar considerations apply to TBS and body composition analysis (19,29,93)

9.5. Integration into Fracture Risk Prediction Models

TBS has been successfully incorporated into FRAX® as an adjustment factor, the most mature example of imaging biomarker integration into a validated clinical risk tool.(19,29) Beyond TBS, integration of CT-derived vBMD, MRI-based bone marrow biomarkers, HR-pQCT microarchitectural parameters, and AI-extracted imaging features into FRAX or next-generation risk models remains active research; UTE-MRI collagen-bound water proton density correlates with FRAX scores in preliminary studies, though confirmation in larger prospective cohorts is required.(21) Machine learning feature selection offers a principled approach to identifying independently predictive biomarkers, but dataset heterogeneity, input feature standardization gaps, and translational barriers between research and clinical imaging environments remain significant obstacles.(29)

9.6. Toward Personalized and Preventive Bone Health Imaging

The convergence of advanced imaging, AI, and multi-omics data is driving precision osteoporosis medicine, where fracture risk assessment and treatment selection are tailored to the individual's complete biological and imaging profile. Opportunistic CT screening is the most immediately scalable preventive strategy: more than half of all osteoporotic fractures occur in individuals who have never undergone formal bone density testing (26,90), and systematic AI-enabled BMD extraction from existing clinical CT volumes could substantially narrow this diagnostic gap without additional patient burden or radiation. Radiogenomics, integrating imaging biomarkers with polygenic risk scores for BMD and fracture susceptibility, offers the possibility of identifying elevated lifetime fracture risk before clinical bone loss is apparent, enabling truly preventive intervention. (26,29)

Emerging imaging technologies hold particular promise: dark-field X-ray imaging (AUC ~0.80 for osteoporotic vs. non-osteoporotic bone ex vivo; Gassert et al., 2023) (28), UTE-MRI (non-ionizing cortical matrix integrity assessment) (94), and REMS (portable, radiation-free DXA alternative under active validation).(91) Addressing the global diagnostic gap also requires confronting economics: osteoporotic fractures cost approximately $57 billion annually in the US and £4 billion in the UK.(26), providing a compelling rationale for investment in esarlier detection, though cost-effectiveness analyses for emerging modalities remain limited and will be essential for health system adoption alongside technical performance data. (26)

10. Reference

1. Dawson-Hughes B, Tosteson ANA, Melton LJ, Baim S, Favus MJ, Khosla S, et al. Implications of absolute fracture risk assessment for osteoporosis practice guidelines in the USA. Osteoporosis International. 2008;19(4):449–58. doi:10.1007/s00198-008-0559-5

2. Silverman SL, Calderon AD. The utility and limitations of FRAX: A US perspective. Current Osteoporosis Reports. Current Medicine Group LLC 1; 2010. p. 192–7. doi:10.1007/s11914-010-0032-1 PubMed PMID: 20811963.
3. Estrada K, Styrkarsdottir U, Evangelou E, Hsu YH, Duncan EL, Ntzani EE, et al. Genome-wide meta-analysis identifies 56 bone mineral density loci and reveals 14 loci associated with risk of fracture. Nat Genet. 2012 May;44(5):491–501. doi:10.1038/ng.2249 PubMed PMID: 22504420.
4. van Geel TACM, van Helden S, Geusens PP, Winkens B, Dinant GJ. Clinical subsequent fractures cluster in time after first fractures. Ann Rheum Dis. 2009 Jan 1;68(1):99–102. doi:10.1136/ard.2008.092775
5. Burghardt AJ, Link TM, Majumdar S. High-resolution computed tomography for clinical imaging of bone microarchitecture. In: Clinical Orthopaedics and Related Research. Springer New York LLC; 2011. p. 2179–93. doi:10.1007/s11999-010-1766-x
6. Krug R, Burghardt AJ, Majumdar S, Link TM. High-Resolution Imaging Techniques for the Assessment of Osteoporosis. Radiologic Clinics of North America. 2010. p. 601–21. doi:10.1016/j.rcl.2010.02.015 PubMed PMID: 20609895.
7. Link TM. Radiology of Osteoporosis. Canadian Association of Radiologists Journal. 2016;67(1):28–40. doi:https://doi.org/10.1016/j.carj.2015.02.002
8. Oei L, Koromani F, Rivadeneira F, Zillikens MC, Oei EHG. Quantitative imaging methods in osteoporosis. Quantitative Imaging in Medicine and Surgery. AME Publishing Company; 2016. p. 680–98. doi:10.21037/qims.2016.12.13
9. Pezzuti IL, Kakehasi AM, Filgueiras MT, De Guimarães JA, De Lacerda IAC, Silva IN. Imaging methods for bone mass evaluation during childhood and adolescence: An update. Journal of Pediatric Endocrinology and Metabolism. Walter de Gruyter GmbH; 2017. p. 485–97. doi:10.1515/jpem-2016-0252 PubMed PMID: 28328530.
10. Twilt M, Pradsgaard D, Spannow AH, Horlyck A, Heuck C, Herlin T. Joint cartilage thickness and automated determination of bone age and bone health in juvenile idiopathic arthritis. Pediatr Rheumatol Online J. 2017 Aug 10;15(1):63. doi:10.1186/s12969-017-0194-9 PubMed PMID: 28797267.
11. YiLdiRiM Y, Tolun A, Tüysüz B. The phenotype caused by PYCR1 mutations corresponds to geroderma osteodysplasticum rather than autosomal recessive cutis laxa type 2. Am J Med Genet A. 2011 Jan;155(1):134–40. doi:10.1002/ajmg.a.33747 PubMed PMID: 21204221.
12. Manhard MK, Nyman JS, Does MD. Advances in imaging approaches to fracture risk evaluation. Translational Research. Mosby Inc.; 2017. p. 1–14. doi:10.1016/j.trsl.2016.09.006 PubMed PMID: 27816505.
13. Costantino F, Gazzotti S, Sassi R, Aparisi Gómez MP, Bazzocchi A. The evolution of CT imaging in metabolic bone disease assessment. International Journal of Bone Fragility. 2025 Oct 1;5(2):40–5. doi:10.57582/ijbf.250502.040
14. Ateeq M, Vergani LM, Buccino F. Integration of Multi-Scale Predictive Tools of Bone Fragility: A Structural and Material Property Perspective. Materials. Multidisciplinary Digital Publishing Institute (MDPI); 2025. doi:10.3390/ma18194639
15. Sollmann N, Kirschke JS, Kronthaler S, Boehm C, Dieckmeyer M, Vogele D, et al. Imaging of the Osteoporotic Spine - Quantitative Approaches in Diagnostics and for the Prediction of the Individual Fracture Risk. RoFo Fortschritte auf dem Gebiet der Rontgenstrahlen und der Bildgebenden Verfahren. Georg Thieme Verlag; 2022. p. 1088–99. doi:10.1055/a-1770-4626 PubMed PMID: 35545103.
16. Casciaro S, Conversano F, Pisani P, Muratore M. New perspectives in echographic diagnosis of osteoporosis on hip and spine. Clinical Cases in Mineral and Bone Metabolism. 2015;12(2):142–50.
17. Xiongfeng T, Cheng Z, Meng H, Chi M, Deming G, Huan Q, et al. One Novel Phantom-Less Quantitative Computed Tomography System for Auto-Diagnosis of Osteoporosis Utilizes Low-Dose Chest Computed Tomography Obtained for COVID-19 Screening. Front Bioeng Biotechnol. 2022 Jun 28;10. doi:10.3389/fbioe.2022.856753
18. Sidhu K, Ali B, Burt LA, Boyd SK, Khan A. Spectrum of microarchitectural bone disease in inborn errors of metabolism: A cross-sectional, observational study. Orphanet J Rare Dis. 2020 Sep 16;15(1). doi:10.1186/s13023-020-01521-6 PubMed PMID: 32938479.
19. Gonera-Furman A, Bolanowski M, Jędrzejuk D. Osteosarcopenia—The Role of Dual-Energy X-ray Absorptiometry (DXA) in Diagnostics. Journal of Clinical Medicine. MDPI; 2022. doi:10.3390/jcm11092522
20. Klintström Eva. Image Analysis for Trabecular Bone Properties on Cone-Beam CT Data. Linkopings Universitet; 2017.

21. Liu J, Liao JW, Li W, Chen XJ, Feng JX, Yao L, et al. Assessment of Osteoporosis in Lumbar Spine: In Vivo Quantitative MR Imaging of Collagen Bound Water in Trabecular Bone. Front Endocrinol (Lausanne). 2022 Feb 16;13. doi:10.3389/fendo.2022.801930
22. Muratore M, Conversano F, Casciaro E, Soloperto G, Franchini R, Greco A, et al. AB0624 High correlation between a new ultrasonic method for spinal densitometry and dual x-ray absorptiometry. Ann Rheum Dis. 2014 Apr;72:A980–A980. doi:10.1136/annrheumdis-2013-eular.2946
23. Dallman J, Herda A, Cleary CJ, Morey T, Diederich A, Vopat BG, et al. A Brief Review of the Literature for Published Dual-Energy X-Ray Absorptiometry Protocols for Athletes. Sports Health. SAGE Publications Inc.; 2024. p. 735–43. doi:10.1177/19417381231208204 PubMed PMID: 37953634.
24. Augdal T, Angenete O, Zadig P, Lundestad A, Nordal E, Shi X, et al. The assessment of bone health in children with juvenile idiopathic arthritis; comparison of different imaging-based methods. Pediatric Rheumatology . 2024 Dec 1;22(1). doi:10.1186/s12969-024-01018-7 PubMed PMID: 39210351.
25. Lorente-Ramos R, Azpeitia-Armán J, Muñoz-Hernández A, García-Gómez JM, Díez-Martínez P, Grande-Bárez M. Dual-energy x-ray absorptiometry in the diagnosis of osteoporosis: A practical guide. American Journal of Roentgenology. 2011. p. 897–904. doi:10.2214/AJR.10.5416 PubMed PMID: 21427343.
26. Cheng X, Zhao K, Zha X, Du X, Li Y, Chen S, et al. Opportunistic Screening Using Low-Dose CT and the Prevalence of Osteoporosis in China: A Nationwide, Multicenter Study. Journal of Bone and Mineral Research. 2021 Mar 1;36(3):427–35. doi:10.1002/jbmr.4187 PubMed PMID: 33145809.
27. Löffler MT, Jacob A, Valentinitsch A, Rienmüller A, Zimmer C, Ryang YM, et al. Improved prediction of incident vertebral fractures using opportunistic QCT compared to DXA. Eur Radiol. 2019 Sep 1;29(9):4980–9. doi:10.1007/s00330-019-06018-w PubMed PMID: 30790025.
28. Gassert FT, Urban T, Kufner A, Frank M, Feuerriegel GC, Baum T, et al. Dark-field X-ray imaging for the assessment of osteoporosis in human lumbar spine specimens. Front Physiol. 2023;14. doi:10.3389/fphys.2023.1217007
29. Wang J, Wang Y, Ren J, Li Z, Guo L, Lv J. Emerging applications of feature selection in osteoporosis research: from biomarker discovery to clinical decision support. Journal of Bone and Mineral Research. Oxford University Press; 2025. p. 1106–13. doi:10.1093/jbmr/zjaf105 PubMed PMID: 40747972.
30. Oo WM, Naganathan V, Bo MT, Hunter DJ. Clinical utilities of quantitative ultrasound in osteoporosis associated with inflammatory rheumatic diseases. Quantitative Imaging in Medicine and Surgery. AME Publishing Company; 2018. p. 100–13. doi:10.21037/qims.2018.02.02
31. Chin KY, Ima-Nirwana S. Calcaneal Quantitative Ultrasound as a Determinant of Bone Health Status: What Properties of Bone Does It Reflect? Int J Med Sci. 2013;10(12):1778–83. doi:10.7150/ijms.6765
32. Métrailler A, Hans D, Lamy O, Gonzalez Rodriguez E, Shevroja E. Heel quantitative ultrasound (QUS) predicts incident fractures independently of trabecular bone score (TBS), bone mineral density (BMD), and FRAX: the OsteoLaus Study. Osteoporosis International. 2023 Aug 1;34(8):1401–9. doi:10.1007/s00198-023-06728-4 PubMed PMID: 37154943.
33. Baroncelli GI. Quantitative Ultrasound Methods to Assess Bone Mineral Status in Children: Technical Characteristics, Performance, and Clinical Application. 2008.
34. Guerri S, Mercatelli D, Gómez MPA, Napoli A, Battista G, Guglielmi G, et al. Quantitative imaging techniques for the assessment of osteoporosis and sarcopenia. Quantitative Imaging in Medicine and Surgery. AME Publishing Company; 2018. p. 60–85. doi:10.21037/qims.2018.01.05
35. Steiner B, Dimai HP, Steiner H, Cirar S, Fahrleitner-Pammer A. Prescreening for Osteoporosis With Quantitative Ultrasound in Postmenopausal White Women. Journal of Ultrasound in Medicine. 2019 Jun 1;38(6):1553–9. doi:10.1002/jum.14844 PubMed PMID: 30341956.
36. Wüster P.; Pereira-Lima J.; Schlegel J.; Anstätt K.; Soballa T. C; H. Quantitative ultrasonometry (QUS) for the evaluation of osteoporosis risk: Reference data for various measurement sites, limitations and application possibilities*. Experimental and Clinical Endocrinology & Diabetes. 1998;106(03):277–88. doi:10.1055/s-0029-1211986
37. Li C, Sun J, Yu L. Diagnostic value of calcaneal quantitative ultrasound in the evaluation of osteoporosis in middle-aged and elderly patients. Medicine (United States). 2022 Jan 14;101(2). doi:10.1097/MD.0000000000028325 PubMed PMID: 35029176.
38. Hans Didier and Métrailler A and GRE and LO and SE. Quantitative Ultrasound (QUS) in the Management of Osteoporosis and Assessment of Fracture Risk: An Update. In: Laugier Pascal and Grimal Q, editor. Bone

Quantitative Ultrasound: New Horizons [Internet]. Cham: Springer International Publishing; 2022. p. 7–34. Available from: https://doi.org/10.1007/978-3-030-91979-5_2 doi:10.1007/978-3-030-91979-5_2
39. Cheon H, Choi W, Lee Y, Lee D, Kim J, Kang JH, et al. Assessment of trabecular bone mineral density using quantitative computed tomography in normal cats. Journal of Veterinary Medical Science. 2012;74(11):1461–7. doi:10.1292/jvms.11-0579 PubMed PMID: 22785567.
40. Engelke K, Adams JE, Armbrecht G, Augat P, Bogado CE, Bouxsein ML, et al. Clinical Use of Quantitative Computed Tomography and Peripheral Quantitative Computed Tomography in the Management of Osteoporosis in Adults: The 2007 ISCD Official Positions. Journal of Clinical Densitometry. 2008;11(1):123–62. doi:https://doi.org/10.1016/j.jocd.2007.12.010
41. Manske S, Macdonald H, Nishiyama K, Boyd S, McKay H. Clinical Tools to Evaluate Bone Strength. Clin Rev Bone Miner Metab. 2010 Apr;8:122–34. doi:10.1007/s12018-009-9066-2
42. Panyasantisuk J, Dall'Ara E, Pretterklieber M, Pahr DH, Zysset PK. Mapping anisotropy improves QCT-based finite element estimation of hip strength in pooled stance and side-fall load configurations. Med Eng Phys. 2018;59:36–42. doi:https://doi.org/10.1016/j.medengphy.2018.06.004
43. Lindtner RA, Kampik L, Schmölz W, Enzenberg M, Putzer D, Arora R, et al. HR-pQCT and 3D Printing for Forensic and Orthopaedic Analysis of Gunshot-Induced Bone Damage. Biomedicines. 2025 Jul 1;13(7). doi:10.3390/biomedicines13071742
44. Gazzotti S, Aparisi Gómez MP, Schileo E, Taddei F, Sangiorgi L, Fusaro M, et al. High-resolution peripheral quantitative computed tomography: research or clinical practice? British Journal of Radiology. British Institute of Radiology; 2023. doi:10.1259/bjr.20221016 PubMed PMID: 37195008.
45. Nishiyama KK, Shane E. Clinical imaging of bone microarchitecture with HR-pQCT. Current Osteoporosis Reports. 2013. p. 147–55. doi:10.1007/s11914-013-0142-7 PubMed PMID: 23504496.
46. Van Den Bergh JP, Szulc P, Cheung & AM, Bouxsein & M, Engelke & K, Chapurlat & R, et al. The clinical application of high-resolution peripheral computed tomography (HR-pQCT) in adults: state of the art and future directions [Internet]. doi:10.1007/s00198-021-05999-z/Published
47. Ohs N, Collins CJ, Atkins PR. Validation of HR-pQCT against micro-CT for morphometric and biomechanical analyses: A review. Bone Reports. Elsevier Inc; 2020. doi:10.1016/j.bonr.2020.100711
48. Yu F, Xu Y, Hou Y, Lin Y, Jiajue R, Jiang Y, et al. Age-, Site-, and Sex-Specific Normative Centile Curves for HR-pQCT-Derived Microarchitectural and Bone Strength Parameters in a Chinese Mainland Population. Journal of Bone and Mineral Research. 2020 Nov 1;35(11):2159–70. doi:10.1002/jbmr.4116 PubMed PMID: 32564403.
49. Flehr A, Källgård J, Alvén J, Lagerstrand K, Papalini E, Wheeler M, et al. Development of a novel method to measure bone marrow fat fraction in older women using high-resolution peripheral quantitative computed tomography. Osteoporosis International. 2022 Jul 1;33(7):1545–56. doi:10.1007/s00198-021-06224-7 PubMed PMID: 35113175.
50. Hsu PC, Luzhbin D, Shih TY, Wu J. Diagnosis of Osteoporosis by Quantifying Volumetric Bone Mineral Density of Lumbar Vertebrae Using Abdominal CT Images and Two-Compartment Model. Healthcare (Switzerland). 2023 Feb 1;11(4). doi:10.3390/healthcare11040556
51. Cordes C, Baum T, Dieckmeyer M, Ruschke S, Diefenbach MN, Hauner H, et al. MR-Based Assessment of Bone Marrow Fat in Osteoporosis, Diabetes, and Obesity. Frontiers in Endocrinology. Frontiers Media S.A.; 2016. doi:10.3389/fendo.2016.00074
52. Li X, Schwartz A V. MRI Assessment of Bone Marrow Composition in Osteoporosis. Current Osteoporosis Reports. Springer; 2020. p. 57–66. doi:10.1007/s11914-020-00562-x PubMed PMID: 31955352.
53. Bae WC, Patil S, Biswas R, Li S, Chang EY, Statum S, et al. Magnetic resonance imaging assessed cortical porosity is highly correlated with μCT porosity. Bone. 2014;66:56–61. doi:10.1016/j.bone.2014.06.004 PubMed PMID: 24928498.
54. Shen W, Gong X, Weiss J, Jin Y. Comparison among T1-weighted magnetic resonance imaging, modified dixon method, and magnetic resonance spectroscopy in measuring bone marrow fat. J Obes. 2013;2013. doi:10.1155/2013/298675 PubMed PMID: 23606951.
55. D Schellinger, C. S. Lin, J. Lim, H. G. Hatipoglu, J. C. Pezzullo, A. J. Singer. Bone Marrow Fat and Bone Mineral Density on Proton MR Spectroscopy and Dual-Energy X-Ray Absorptiometry: Their Ratio as a New Indicator of Bone Weakening. AJR Am J Roentgenol. 2004 Dec. doi:0361–803X/04/1836–1761

56. Jones BC, Lee H, Cheng CC, al Mukaddam M, Song HK, Snyder PJ, et al. MRI Quantification of Cortical Bone Porosity, Mineralization, and Morphologic Structure in Postmenopausal Osteoporosis. Radiology. 2023 Apr 1;307(2). doi:10.1148/radiol.221810 PubMed PMID: 36692396.
57. Metwally MI, Almalki YE, Khalil MF, Alsowey AM, Tantawy HIA, Hamed MG, et al. Quantitative MRI Dixon signal drop and fat fraction for differentiating bone marrow lesions: a two-center prospective analysis. Eur Radiol Exp. 2025 Dec 1;9(1). doi:10.1186/s41747-025-00615-9 PubMed PMID: 40928596.
58. Li X, Kuo D, Schafer AL, Porzig A, Link TM, Black D, et al. Quantification of vertebral bone marrow fat content using 3 Tesla MR spectroscopy: Reproducibility, vertebral variation, and applications in osteoporosis. Journal of Magnetic Resonance Imaging. 2011 Apr;33(4):974–9. doi:10.1002/jmri.22489 PubMed PMID: 21448966.
59. Pei XJ, Lian YF, Yan YC, Jiang T, Liu AJ, Shi QL, et al. Fat fraction quantification of lumbar spine: Comparison of t1-weighted two-point dixon and single-voxel magnetic resonance spectroscopy in diagnosis of multiple myeloma. Diagnostic and Interventional Radiology. 2020 Sep 1;26(5):492–7. doi:10.5152/dir.2020.19401 PubMed PMID: 32755881.
60. Wong KK, Piert M. Dynamic bone imaging with 99mTc-labeled diphosphonates and 18F-NaF: mechanisms and applications. J Nucl Med. 2013 Apr 1;54(4):590–9. doi:10.2967/JNUMED.112.114298 PubMed PMID: 23482667.
61. Czernin J, Satyamurthy N, Schiepers C. Molecular mechanisms of bone 18F-NaF deposition. Journal of Nuclear Medicine. 2010. p. 1826–9. doi:10.2967/jnumed.110.077933 PubMed PMID: 21078790.
62. Tzolos E, Dweck MR. 18F-Sodium Fluoride (18F-NaF) for Imaging Microcalcification Activity in the Cardiovascular System. Arterioscler Thromb Vasc Biol. 2020 Jul 1;40(7):1620–6. doi:10.1161/ATVBAHA.120.313785 PubMed PMID: 32375543.
63. Ahuja K, Sotoudeh H, Galgano SJ, Singh R, Gupta N, Gaddamanugu S, et al. 18F-Sodium Fluoride PET: History, Technical Feasibility, Mechanism of Action, Normal Biodistribution, and Diagnostic Performance in Bone Metastasis Detection Compared with Other Imaging Modalities. J Nucl Med Technol. 2020 Mar 1;48(1):9–16. doi:10.2967/JNMT.119.234336 PubMed PMID: 31811067.
64. Blake GM, Puri T, Siddique M, Frost ML, Moore AEB, Fogelman I. Site specific measurements of bone formation using [18F] sodium fluoride PET/CT. Quantitative Imaging in Medicine and Surgery. AME Publishing Company; 2018. p. 47–59. doi:10.21037/qims.2018.01.02
65. de Ruiter RD, Zwama J, Raijmakers PGHM, Yaqub M, Burchell GL, Boellaard R, et al. Validation of quantitative [18F]NaF PET uptake parameters in bone diseases: a systematic review. Annals of Nuclear Medicine. Springer; 2024. doi:10.1007/s12149-024-01991-9 PubMed PMID: 39729191.
66. Mick CG, James T, Hill JD, Williams P, Perry M. Molecular imaging in oncology:18F-sodium fluoride PET imaging of osseous metastatic disease. American Journal of Roentgenology. American Roentgen Ray Society; 2014. p. 263–71. doi:10.2214/AJR.13.12158 PubMed PMID: 25055258.
67. Park PSU, Raynor WY, Sun Y, Werner TJ, Rajapakse CS, Alavi A. 18F-sodium fluoride pet as a diagnostic modality for metabolic, autoimmune, and osteogenic bone disorders: Cellular mechanisms and clinical applications. International Journal of Molecular Sciences. MDPI; 2021. doi:10.3390/ijms22126504 PubMed PMID: 34204387.
68. Jadvar H, Desai B, Conti PS. Sodium 18F-fluoride PET/CT of bone, joint, and other disorders. In: Seminars in Nuclear Medicine. W.B. Saunders; 2015. p. 58–65. doi:10.1053/j.semnuclmed.2014.07.008 PubMed PMID: 25475379.
69. Ulusoy OL, Server S, Yesilova M, Inan N. Whole-body PET/MRI to detect bone metastases: comparison of the diagnostic performance of the sequences. Radiol Oncol. 2024 Dec 1;58(4):494–500. doi:10.2478/raon-2024-0062 PubMed PMID: 39608007.
70. Kogan F, Broski SM, Yoon D, Gold GE. Applications of PET-MRI in musculoskeletal disease. Journal of Magnetic Resonance Imaging. 2018 Jul 1;48(1):27–47. doi:10.1002/jmri.26183 PubMed PMID: 29969193.
71. Puri T, Moore AE, Mahajan A, McWilliam A, Vrist MH, Blake GM. Editorial: Quantitative [18F]NaF PET in metastatic and metabolic bone diseases. Frontiers in Nuclear Medicine. Frontiers Media SA; 2023. doi:10.3389/fnume.2023.1343913
72. Velez EM, Desai B, Jadvar H. Treatment Response Assessment of Skeletal Metastases in Prostate Cancer with 18F-NaF PET/CT. Nucl Med Mol Imaging. 2019 Aug 1;53(4):247–52. doi:10.1007/s13139-019-00601-1

73. Taralli S, Caldarella C, Lorusso M, Scolozzi V, Altini C, Rubini G, et al. Comparison between 18F-FDG and 18F-NaF PET imaging for assessing bone metastases in breast cancer patients: a literature review. Clin Transl Imaging. 2020 Apr 1;8(2):65–78. doi:10.1007/S40336-020-00363-3
74. Beheshti M, Mottaghy FM, Payche F, Behrendt FFF, Van den Wyngaert T, Fogelman I, et al. 18F-NaF PET/CT: EANM procedure guidelines for bone imaging. Eur J Nucl Med Mol Imaging. 2015 Oct 4;42(11):1767–77. doi:10.1007/s00259-015-3138-y PubMed PMID: 26201825.
75. Kawaguchi M, Tateishi U, Shizukuishi K, Suzuki A, Inoue T. 18F-fluoride uptake in bone metastasis: morphologic and metabolic analysis on integrated PET/CT. Annals of Nuclear Medicine 2010 24:4. 2010 Mar 24;24(4):241–7. doi:10.1007/S12149-010-0363-0 PubMed PMID: 20333485.
76. Sarikaya Ismet, Elgazzar Abdelhamid H., Sarikaya Ali, Alfeeli Mahmoudb. Normal bone and soft tissue distribution of fluorine-18-sodium fluoride and artifacts on 18F-NaF PET/CT bone scan. Nucl Med Commun. 2017 Oct. doi:10.1097/MNM.0000000000000720
77. Pisani P. Screening and early diagnosis of osteoporosis through X-ray and ultrasound based techniques. World J Radiol. 2013;5(11):398. doi:10.4329/wjr.v5.i11.398
78. Guerri S, Mercatelli D, Gómez MPA, Napoli A, Battista G, Guglielmi G, et al. Quantitative imaging techniques for the assessment of osteoporosis and sarcopenia. Quantitative Imaging in Medicine and Surgery. AME Publishing Company; 2018. p. 60–85. doi:10.21037/qims.2018.01.05
79. Malekzadeh M, Asadi M, Abbasi-Rad S, Abolghasemi J, Hamidi Z, Talebi M, et al. MDCT-QCT, QUS, and DXA in healthy adults: An intermodality comparison. Med J Islam Repub Iran. 2019. doi:10.34171/mjiri.33.156
80. Shepherd JA, Schousboe JT, Broy SB, Engelke K, Leslie WD. Executive Summary of the 2015 ISCD Position Development Conference on Advanced Measures From DXA and QCT: Fracture Prediction Beyond BMD. Journal of Clinical Densitometry. 2015;18(3):274–86. doi:10.1016/j.jocd.2015.06.013 PubMed PMID: 26277847.
81. Sornay-Rendu E, Boutroy S, Duboeuf F, Chapurlat RD. Bone Microarchitecture Assessed by HR-pQCT as Predictor of Fracture Risk in Postmenopausal Women: The OFELY Study. Journal of Bone and Mineral Research. 2017 Jun 1;32(6):1243–51. doi:10.1002/jbmr.3105 PubMed PMID: 28276092.
82. Collins CJ, Atkins PR, Ohs N, Blauth M, Lippuner K, Müller R. Clinical observation of diminished bone quality and quantity through longitudinal HR-pQCT-derived remodeling and mechanoregulation. Sci Rep. 2022 Dec 1;12(1). doi:10.1038/s41598-022-22678-z PubMed PMID: 36289391.
83. Li J, She BY, He ML, Yuan C, Li N. Advances in imaging examination of bone density and bone quality. Endokrynologia Polska. Via Medica; 2025. p. 29–39. doi:10.5603/ep.100805 PubMed PMID: 40071797.
84. Pickhardt PJ, Nguyen T, Perez AA, Graffy PM, Jang S, Summers RM, et al. Improved CT-based Osteoporosis Assessment with a Fully Automated Deep Learning Tool. Radiol Artif Intell. 2022 Sep 1;4(5). doi:10.1148/ryai.220042
85. Pizza Alessia; Pedullà Martina; Albano Domenico; Sconfienza Luca Maria; Messina Carmelo ICB. DXA: New Concepts and Tools Beyond Bone Mineral Density. Semin Musculoskelet Radiol. 2024;28(05):528–38. doi:10.1055/s-0044-1788579
86. Wang J, Zhou S, Chen S, He Y, Gao H, Yan L, et al. Prediction of osteoporosis using radiomics analysis derived from single source dual energy CT. BMC Musculoskelet Disord. 2023 Dec 1;24(1). doi:10.1186/s12891-022-06096-w PubMed PMID: 36750927.
87. Chen B, Cui J, Li C, Xu P, Xu G, Jiang J, et al. Application of radiomics model based on lumbar computed tomography in diagnosis of elderly osteoporosis. Journal of Orthopaedic Research. 2024 Jun 1;42(6):1356–68. doi:10.1002/jor.25789 PubMed PMID: 38245854.
88. Chen-Mayer HH, Fuld MK, Hoppel B, Judy PF, Sieren JP, Guo J, et al. Standardizing CT lung density measure across scanner manufacturers. Med Phys. 2017 Mar 1;44(3):974–85. doi:10.1002/MP.12087 PubMed PMID: 28060414.
89. Schmeel FC, Vomweg T, Träber F, Gerhards A, Enkirch SJ, Faron A, et al. Proton density fat fraction MRI of vertebral bone marrow: Accuracy, repeatability, and reproducibility among readers, field strengths, and imaging platforms. Journal of Magnetic Resonance Imaging. 2019 Dec 1;50(6):1762–72. doi:10.1002/JMRI.26748;CTYPE:STRING:JOURNAL PubMed PMID: 30980694.
90. Bone Mineral Density, Bone Micro-Architecture Evolution After Kidney Transplantation: A Prospective Cohort Study - ATC Abstracts [Internet]. [cited 2026 Apr 7]. Available from:

https://atcmeetingabstracts.com/abstract/bone-mineral-density-bone-micro-architecture-evolution-after-kidney-transplantation-a-prospective-cohort-study/
91. Zambito K, Kushchayeva Y, Bush A, Pisani P, Kushchayeva S, Peters M, et al. Proposed practice parameters for the performance of radiofrequency echographic multispectrometry (REMS) evaluations. doi:10.1302/2633-1462
92. Chung YS, Kim W. General Endocrinology SUN-814 Artificial Intelligence Image Analysis Of Osteoporosis In Dual-energy X-ray Absorptiometry-Preset Data [Internet]. doi:10.1210/jendso/bvaf149
93. Imoto Y, Inui T, Matsui K, Watanabe Y, Igari T, Takeuchi S, et al. Deep Learning Model for Osteoporosis Screening From Chest Radiographs: A Multicenter Analysis of External Robustness and Model Calibration. Cureus. 2025 Aug 6. doi:10.7759/cureus.89446
94. Wan L, Zhao W, Ma Y, Jerban S, Searleman AC, Carl M, et al. Fast quantitative 3D ultrashort echo time MRI of cortical bone using extended cones sampling. Magn Reson Med. 2019 Jul 1;82(1):225–36. doi:10.1002/mrm.27715 PubMed PMID: 30821032.